Size effects in single asperity frictional contacts

Deshpande, V. S.; Balint, D. S.; Needleman, A.; Van der Giessen, E.

Published in:
Modelling and Simulation in Materials Science and Engineering

DOI:
10.1088/0965-0393/15/1/S09

Publication date:
2007

INSTITUTE OF PHYSICS PUBLISHING MODELLING AND SIMULATION IN MATERIALS SCIENCE AND ENGINEERING

Modelling Simul. Mater. Sci. Eng. **15** (2007) S97–S108 doi:10.1088/0965-0393/15/1/S09

Size effects in single asperity frictional contacts

V S Deshpande[1], D S Balint[1], A Needleman[2] and E Van der Giessen[3]

[1] Department of Engineering, Cambridge University, Trumpington Street, Cambridge CB2 1PZ, UK
[2] Division of Engineering, Brown University, Providence, RI 02912, USA
[3] Department of Applied Physics, University of Groningen, Nyenborgh 4, 9747 AG Groningen, The Netherlands

Received 1 June 2006, in final form 31 August 2006
Published 7 December 2006
Online at stacks.iop.org/MSMSE/15/S97

Abstract

Two sets of indentation and sliding discrete dislocation plasticity analyses are carried out to investigate the initiation of frictional sliding between a rigid asperity and a single crystal film. Most calculations are carried out for sinusoidal asperities, but for comparison purposes some results are presented for wedge-shaped asperities. In one set of calculations the friction coefficient is evaluated from separate indentation and sliding calculations while in another set the indentation and sliding processes are carried out sequentially. Both sets of friction calculations predict a similar friction stress versus contact size relation with the friction stress dominated by adhesion at small contact sizes, being plasticity governed at large contact sizes and being strongly size dependent at intermediate values of the contact size. Remarkably, the predicted values of the friction coefficient are similar for both sets of calculations even though the predicted deformation fields and dislocation structures differ significantly.

(Some figures in this article are in colour only in the electronic version)

1. Introduction

Frictional sliding is a complicated process generally involving large deformation of asperities having a wide range of size scales. The classical Amontons–Coulomb description of friction states that the shear force along an interface is proportional to the normal force, with the proportionality constant being the coefficient of friction μ. However, experiments have shown that friction is both time-and slip distance-dependent (e.g. Dieterich [1], Ruina [2], Prakash and Clifton [3], Gearing *et al* [4]). In a more general context it is the evolution of the sliding force and its dependence on the normal force that characterizes frictional sliding.

In their classical work Bowden and Tabor [5] wrote the frictional force as $F_f = \tau_f A_t$, where τ_f is the contact shear stress and A_t is the true area of contact. The main contribution to the normal force dependence arises from its effect on the true area of contact, both through the number of asperities in contact and the evolution of the asperity shapes, although there can also be an effect of normal force for a single asperity.

Here, we confine attention to frictional sliding along an interface between a ductile single crystal and a hard solid that is idealized as rigid. Furthermore, we confine attention to a single asperity with an idealized shape. When the asperity contact size is sufficiently small, conventional continuum theories of plasticity fail to predict the response and discrete dislocation effects come into play. Indeed, Kuhlmann–Wilsdorf [6] noted in 1981 that the plastic response of an asperity would be size dependent when the asperity size was of the order of the dislocation source spacing. In a pioneering study, Polonsky and Keer [7] used discrete dislocation plasticity to model elastic–plastic deformation of micro-contacts on scales too small to apply conventional continuum plasticity. Their analysis revealed that when the asperity size becomes comparable to the dislocation source spacing, the asperities can sustain considerably greater loads than those predicted by continuum plasticity.

Hurtado and Kim [8, 9] analysed frictional size scale effects using a discrete dislocation model and found three regimes in the variation of τ_f with contact size. For relatively large contacts, τ_f is equal to the Peierls stress while for very small contacts τ_f is equal to the theoretical shear strength of the solid. The transition between these two regimes is governed by the stress to nucleate a dislocation loop at the edge of the contact, and Hurtado and Kim [8, 9] obtained a scaling of τ_f with the contact size a as $\tau_f \propto a^{-1/2}$. Arguing that the size of the interface zone over which plasticity occurs scales with the contact size, Bhushan and Nosonovsky [10] obtained a similar scaling. The analyses of sliding of Deshpande *et al* [11] presume that dislocations are generated by Frank–Read sources in the bulk, not at the surface as in the model of Hurtado and Kim [8, 9]. Nevertheless, a similar scaling with asperity size was obtained.

In the present study, the effect of size on the single asperity friction coefficient is explored. In one set of calculations, an indentation calculation is carried out to determine the contact area versus applied normal load relation followed by an independent calculation of the initiation of sliding, as in [11], using a cohesive shear traction–displacement relation on the contact area determined by the indentation calculation. Such calculations only approximately represent the combination of sliding with an imposed normal pressure, since for example the effect of the change in surface shape due to the normal loading is not accounted for in the sliding calculations. In the second set of calculations the analysis of sliding starts from the stress state and dislocation distribution induced by the normal loading. The predictions of these two sets of calculations are compared.

2. Discrete dislocation formulation

We analyse the plane strain indentation and sliding of two-dimensional single crystal films on rigid substrates (figure 1). The crystal is taken to be elastically isotropic with Young's modulus $E = 70\,\text{GPa}$ and Poisson's ratio $\nu = 0.33$. It has three slip systems at angles $\phi^{(\alpha)} = \pm 54.7^\circ, 90.0^\circ$ relative to the free top surface. Plasticity is a result of the collective motion of edge dislocations with Burgers vector magnitude $b = 0.25\,\text{nm}$. The dislocations are treated as line singularities in a linear elastic continuum with their motion and evolution being governed by a set of constitutive rules. Superposition is used to calculate the stress and deformation state at each stage [12]. This method involves the ($\tilde{}$) field caused by dislocations, calculated analytically from the linear isotropic elastic dislocation fields, and a smooth image field ($\hat{}$) that corrects the solutions to satisfy the boundary conditions. We use the finite element method to solve the linear elastic boundary value problem for the ($\hat{}$) image fields.

The computations start with a dislocation-free crystal. This crystal has sources with a density $\rho_{\text{src}} = 48\,\mu\text{m}^{-2}$ and obstacles with a density $\rho_{\text{obs}} = 98\,\mu\text{m}^{-2}$ that are randomly placed on the slip planes spaced $100b$ apart. The sources nucleate a dislocation dipole when the

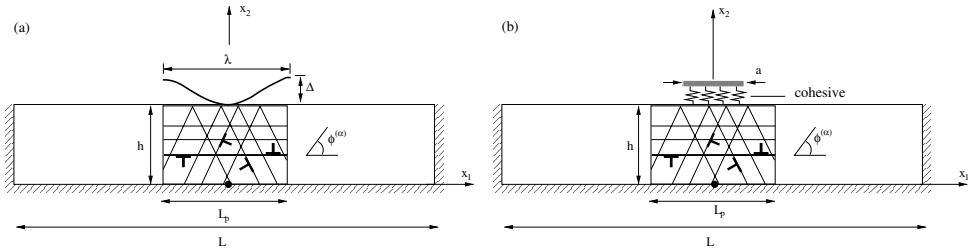

Figure 1. Sketches of the (*a*) indentation and (*b*) sliding boundary value problems analysed to determine the friction for single asperity contact. The origin of the coordinate system employed is marked as a filled-in circle (●) in (*a*) and (*b*).

resolved shear stress on the source exceeds τ_{nuc} over a period $t_{\text{nuc}} = 10\,\text{ns}$. In the computations here, the source strengths have a Gaussian distribution with an average value $\bar{\tau}_{\text{nuc}} = 50\,\text{MPa}$ and a standard deviation $\Delta\tau_{\text{nuc}} = 10\,\text{MPa}$.

Glide of dislocation I is controlled by the Peach–Koehler force, whose component in the slip direction is $f^{(I)}$ and the glide velocity is given by $v^{(I)} = f^{(I)}/B$ with $B = 10^{-4}\,\text{Pas}$. When a dislocation meets an obstacle, it is pinned there and released only when the Peach–Koehler force exceeds $b\tau_{\text{obs}}$, where $\tau_{\text{obs}} = 150\,\text{MPa}$ is the obstacle strength. If two dislocations of opposite sign come within a critical distance $L_e = 6b$ on a slip plane, they annihilate.

2.1. Geometry and boundary conditions

Calculations were performed for films of thicknesses $h = 2, 10\,\mu\text{m}$ and $50\,\mu\text{m}$ (figure 1). Two asperity shapes are considered: (i) a sinusoidal asperity (figure 1(*a*)) with a wavelength λ and amplitude $\Delta = 0.5\,\mu\text{m}$; and (ii), as in Balint *et al* [13], a wedge-like asperity with a wedge angle ω (measured with respect to the top surface of the film). Dislocation activity in a film of length $L = 1000\,\mu\text{m}$ was restricted to a process region of length $L_p = 50\,\mu\text{m}$. The calculations were terminated before dislocations reached the boundaries $x_1 = \pm L_p/2$ and thus the effect of the process region is to restrict the extent to which the indentation or sliding calculations were carried out. Two sets of calculations are performed; indentation calculations and sliding calculations.

In the indentation calculations, the contact between the rigid asperity and the film is based on the deformed film surface. Perfect sticking is assumed as soon as the asperity comes in contact with the film; hence, the rate boundary conditions applied are

$$\dot{u}_1 = 0, \qquad \dot{u}_2 = -\dot{\delta} \quad \text{on} \quad S_{\text{contact}}, \tag{1}$$

where S_{contact} denotes the portion of the deformed surface in contact with the asperity and $\dot{\delta} = 0.4\,\text{ms}^{-1}$ is the indentation rate. The other boundary conditions are

$$\dot{u}_1 = \dot{u}_2 = 0, \qquad \text{on} \quad x_1 = \pm L/2 \quad \text{and on} \quad x_2 = 0, \tag{2}$$

and $\dot{T}_1 = \dot{T}_2 = 0$ on $x_2 = h \notin S_{\text{contact}}$. Here, $T_i = \sigma_{ij} n_j$ is the surface traction on a surface with outward normal n_j. The applied load is computed as

$$F = -\int_{-L/2}^{L/2} T_2(x_1, h)\,\mathrm{d}x_1 \tag{3}$$

to give the indentation pressure p defined by

$$p \equiv \frac{F}{a}, \tag{4}$$

where a is the end-to-end length of the contact region.

In the sliding calculations, adhesion on the contacting surface of length a (figure 1(b)) is modelled via a shear traction versus displacement relation described by

$$T_t = \begin{cases} -\tau_{max}\dfrac{\Delta_t}{\delta_t} & \text{if } |\Delta_t| < \delta_t, \\ -\tau_{max}\text{sign}(\Delta_t) & \text{otherwise,} \end{cases} \tag{5}$$

where $\Delta_t = u_1(x_1, h)$ is the tangential displacement jump across the cohesive surface and $T_t = T_1$ is the shear traction. Again, we specify that $T_1 = T_2 = 0$ on $x_2 = h$ and $|x_1| \geqslant a/2$, i.e. the surface outside the contact region is traction free. The cohesive strength τ_{max} is taken to be 300 MPa and $\delta_t = 0.5$ nm. Deshpande *et al* [11] considered a softening cohesive relation as well as one of the form of equation (5) and found that the initiation of sliding is relatively insensitive to the choice of cohesive relation.

The displacement rates

$$\dot{u}_1 = U, \qquad \dot{u}_2 = 0, \tag{6}$$

are applied on the boundaries $x_1 = \pm L/2$ and $x_2 = 0$ to simulate the relative sliding of the contacting surfaces with $\dot{U}/a = 10^4\ \text{s}^{-1}$. The mean contact shear stress τ is given by

$$\tau = -\frac{1}{a}\int_{-L/2}^{L/2} T_1(x_1, h)\,\text{d}x_1, \tag{7}$$

and the friction coefficient μ is defined as

$$\mu = \frac{\tau}{p}. \tag{8}$$

Two types of sliding calculations are carried out. In one set, the sliding calculations are performed for an initially stress and dislocation-free crystal as in [11]. In the other set of calculations, the traction T_2 on the contact surface caused by the preceding indentation is retained by applying traction boundary conditions. Also, the dislocation structure created by the indentation is present at the start of the sliding calculation. Furthermore, the sticking constraint $\dot{u}_1 = 0$ in the indentation contact region in equation (1) is relaxed and replaced by the shear cohesive law equation (5), as used in the sliding calculations for a dislocation-free crystal.

The finite element mesh was highly refined in a $30\,\mu\text{m} \times h$ region around the centre of the contact area and usually consisted of 180×100 bilinear elements with a typical mesh size of about $0.01\,\mu$m in a central $1\,\mu\text{m} \times 1\,\mu$m region. A time step of $\Delta t = 0.5$ ns is used in all the calculations in order to accurately resolve the dislocation dynamics.

3. Indentation

The indentation pressure p versus contact length a response is plotted in figures 2(a) and (b) for indentation of $h = 50\,\mu$m, $10\,\mu$m and $2\,\mu$m films by rigid sinusoidal asperities with an amplitude $\Delta = 0.5\,\mu$m and wavelengths $\lambda = 20\,\mu$m and $10\,\mu$m, respectively. These curves are obtained by cross-plotting $p = F(\delta)/a(\delta)$ and $a(\delta)$. For the $h = 50$ and $10\,\mu$m films, p first increases rapidly with increasing a and then tends to level off. In contrast, p continues to increase with increasing a for the thinner $h = 2\,\mu$m film as the plastic zone under the indenter gets constrained by the rigid substrate.

Increasing the sharpness of the asperity, i.e. increasing the ratio Δ/λ, increases the indentation pressure for a given contact length a for the thicker $h = 50$ and $10\,\mu$m films. This is due to the fact that a larger indentation depth is required for the sharper asperities to achieve the same contact length. However, the trend is opposite for the $h = 2\,\mu$m films.

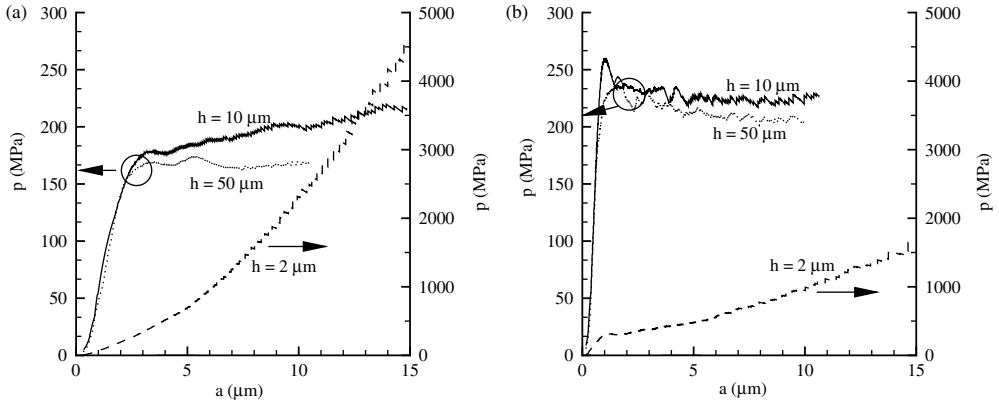

Figure 2. The indentation pressure p versus contact length a relation for indentation with sinusoidal-shaped asperities of amplitude $\Delta = 0.5\,\mu$m and wavelengths (a) $\lambda = 20\,\mu$m and (b) $\lambda = 10\,\mu$m. Results are shown for three values of film thickness h.

As in [13], this difference is associated with the fact that significant material pile-up occurs during indentation of the thin $h = 2\,\mu$m films when dislocation glide is restricted by the rigid substrate while some material sink-in occurs for the thicker films.

4. Single asperity sliding and friction

4.1. Sliding from a stress and dislocation free state

As in Deshpande *et al* [11], we analyse the boundary value problem sketched in figure 1(b) for an initially dislocation-free crystal. Computed curves of shear stress τ defined in equation (7) versus applied displacement, U, are shown in figure 3(a) for the $h = 10\,\mu$m film and for selected values of the contact length a. The value of τ first increases approximately linearly with U and then reaches a plateau. In general the shear stresses are greater for the smaller contacts. For the smallest contact ($a = 0.04\,\mu$m), no dislocation activity occurs before the cohesive strength $\tau_{\max} = 300$ MPa is attained.

The friction stress, τ_{ave}, is defined as the average value of τ over the range $0.015\,\mu\text{m} \leqslant U \leqslant 0.02\,\mu$m. For the largest values of a, τ has attained a steady-state value for displacements in this range. The τ–U curve depends on the specific distribution of dislocation sources and obstacles and not just on the densities. Here, calculations were carried out for two realizations; the values obtained for the two realizations differed by less than 5 % in all cases and the values of τ_{ave} reported are mean values. The relation between friction stress τ_{ave} and contact size a, shown in figure 3(b), appears to be insensitive to the film thickness h over the range considered here because, as in [11], the plastic zone penetrates to only about $1\,\mu$m under the sliding asperity. This can be contrasted with the indentation response where the plastic zone penetrates deep into the film so that the film thickness can then significantly affect the indentation response.

The qualitative features of the τ_{ave}–a curve, figure 3(b), are similar to those reported by Deshpande *et al* [11]. The curve displays two plateaus: for large contacts ($a \geqslant 10\,\mu$m here), τ_{ave} is approximately independent of a with τ_{ave} approximately equal to the shear flow strength of the single crystal, while for small contacts ($a \leqslant 0.2\,\mu$m), τ_{ave} is equal to the cohesive strength $\tau_{\max}$. In the transition regime, τ_{ave} increases with decreasing a. This size effect arises not only due to size effects that result from the imposed strain gradients and the consequent

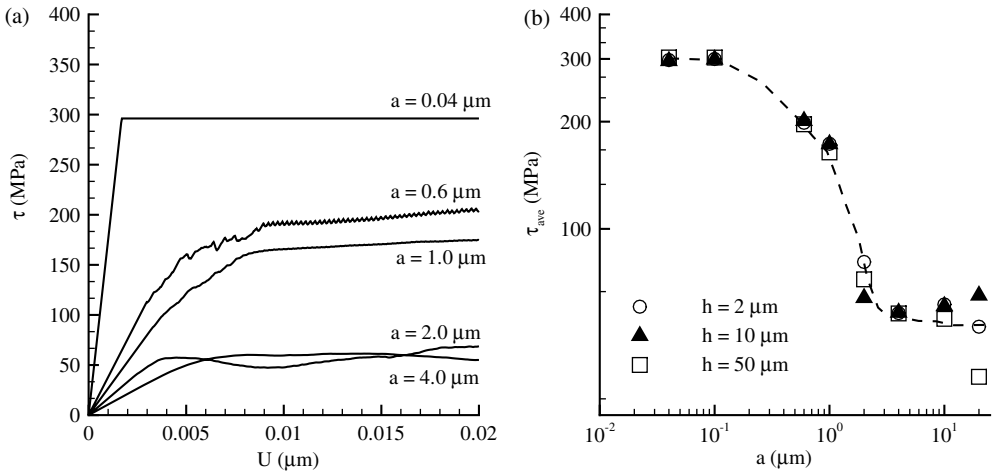

Figure 3. (*a*) Friction stress versus displacement response for the $h = 10\,\mu$m film for selected values of the contact area a. (*b*) The average friction stress τ_{ave} as a function of contact size for three selected values of film thickness h. These results are for sliding with no prior indentation.

build-up of geometrically necessary dislocations but also is a consequence of the discreteness of the dislocation sources and obstacles (see [11]). The form of the dependence of friction stress on contact size in figure 3(*b*) is consistent with the low values of friction stress found experimentally in the surface force apparatus [14], where the contact area is relatively large, and the much larger friction stress values seen for contact with an atomic force microscope tip [15], where the contact area is relatively small. Only very recently have measurements been made in the transition regime and the experimental measurements are in good agreement with a square root dependence on contact size [16].

4.2. Friction predictions for an initially stress and dislocation free crystal

Here, for a given indentation force F, the end-to-end contact length a is obtained by the indentation simulations in section 3. The frictional sliding force τa is then obtained from the sliding simulations presented in section 4.1.

The friction coefficient, $\mu \equiv \tau/p$, at fixed a for the sinusoidal asperity with $\lambda = 20\,\mu$m is shown in figure 4 and obtained from a combination of the results in figures 2(*a*) and 3(*a*) (by dividing $\tau(U)$ by the value of p needed to obtain the specified value of a). The dependence of μ on the sliding displacement U at selected values of contact size a is plotted in figure 4(*a*) for the sinusoidal asperity with wavelength $\lambda = 20\,\mu$m. The coefficient of friction μ increases with increasing U and then attains a steady-state for U greater than about 5 nm. Thus, the mean value, $\mu_{ave} \equiv \tau_{ave}/p$, for a single asperity is attained after very little sliding. The value of μ_{ave} increases with decreasing contact size. The variation of μ_{ave} with a is summarized in figure 4(*b*) for the three film thicknesses: μ_{ave} increases with decreasing contact size for contact sizes $a \leqslant 2\,\mu$m and is essentially independent of contact size for $a > 2\,\mu$m in the two thicker films. The increase in μ_{ave} with decreasing a is a result of the fact that the indentation pressure decreases with contact length for small contact sizes (figure 2(*a*)). As the contact size increases, both the indentation pressure and friction stress τ_{ave} become approximately independent of a for the thicker films and thus μ_{ave} becomes approximately independent of contact size. In contrast, for the $h = 2\,\mu$m film, the indentation pressure continues to increase

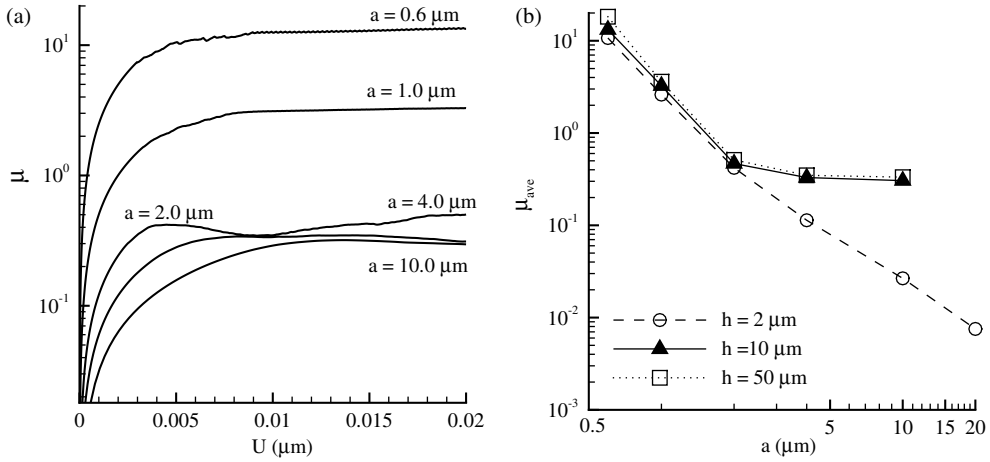

Figure 4. (*a*) The friction coefficient $\mu = \tau/p$ versus sliding displacement U in the $h = 10\,\mu$m film and (*b*) the friction coefficient $\mu_{ave} = \tau_{ave}/p$, where τ_{ave} is the average value of τ over the range $0.015\,\mu\text{m} \leqslant U \leqslant 0.02\,\mu$m, as a function of contact size a. In both (*a*) and (*b*) $\Delta = 0.5\,\mu$m and wavelength $\lambda = 20\,\mu$m. The sliding calculations are carried out for an initially stress and dislocation-free crystal, while the pressure p for each a is the one needed according to figure 2(*a*) to achieve this contact length under indentation.

with increasing a (figure 2) while the friction stress remains approximately constant. Thus, no plateau in the μ_{ave} versus a curve is seen for the $h = 2\,\mu$m films with μ_{ave} decreasing with increasing a for all values of contact size considered here. While the μ_{ave} values for the thick films are similar to those reported as the 'static' friction coefficients for metallic contacts [5], the large contact μ_{ave} values for the $h = 2\,\mu$m film are significantly smaller than most experimental observations. The predicted dependence of μ_{ave} on film thickness remains to be experimentally verified.

Bhushan and Nosonovsky [10] have presented a similar analysis based on scaling relations derived from nonlocal plasticity considerations. In their model, the material length scales that give rise to the size dependence of the contact pressure and friction stress are inputs, whereas in the discrete dislocation simulations the size dependence emerges as a natural outcome, and can be associated with multiple length scales; for example, one length scale associated with geometrically necessary dislocations and/or another length scale associated with the spacings of dislocation sources and obstacles.

The size dependence of the single asperity friction coefficient μ_{ave} for the $h = 10\,\mu$m and $h = 50\,\mu$m films obtained here is consistent with a number of single asperity molecular dynamics studies (see, for example, [17, 18]) but is contrary to the experimental finding that the coefficient of friction decreases with decreasing contact sizes [19]. However, in Ruan and Bhushan [19] the scale dependence of μ was inferred from two separate scratch tests: one with an AFM tip with a 50 nm radius and the other with a 3 mm ball.

4.3. Effect of asperity shape

The variation of the friction coefficient μ_{ave} with contact size is plotted in figure 5(*a*) for the sinusoidal asperity with $\lambda = 10\,\mu$m. A comparison with the results in figure 4(*b*) shows that the contact size dependence of μ_{ave} is reduced for this sharper asperity ($\Delta/\lambda = 0.05$) compared with the $\Delta/\lambda = 0.025$ asperity in figure 4.

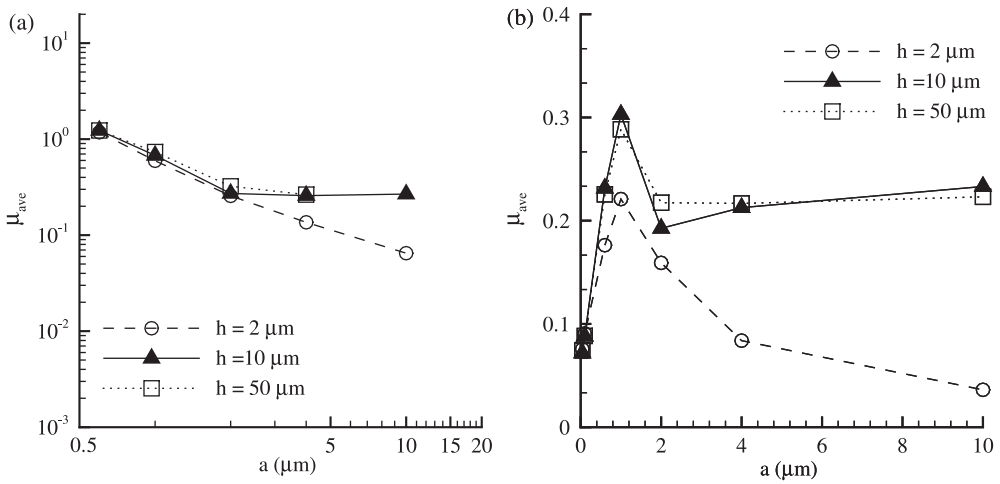

Figure 5. The friction coefficient $\mu_{ave} = \tau_{ave}/p$ as a function of contact size for (*a*) a sinusoidal asperity with $\lambda = 10\,\mu$m and $\Delta = 0.5\,\mu$m and (*b*) a wedge asperity with $\omega = 5^\circ$. The sliding calculations are carried out for an initially stress and dislocation-free crystal.

In order to further explore the effect of asperity shape on the trends shown in figures 4(*b*) and 5(*a*) we consider the friction coefficient for a wedge-like asperity. As in section 4.2, the sliding calculations start from a dislocation and stress-free state. Indentation pressure versus contact length predictions for indentation with a $\omega = 5^\circ$ wedge is given by Balint *et al* [13] for the materials considered here. In these indentation calculations, there is no length scale associated with the indenter geometry, and consistent with a wide body of experimental data (see, for example, a review of the literature in [20]), Balint *et al* [13] showed that the discrete dislocation calculations predict that the indentation pressure decreases with increasing contact size (when the film is thick enough to avoid interaction with the rigid substrate).

The computed values of μ_{ave} for a wedge-like asperity ($\omega = 5^\circ$) for the three film thicknesses are plotted in figure 5(*b*) as a function of the contact size a. The coefficient of friction μ_{ave} decreases with decreasing contact size for contact sizes $a \leqslant 1\,\mu$m and is essentially independent of contact size for larger contact sizes in the two thicker films. For the materials considered here, the large-contact size value of the single asperity friction coefficient is $\mu_{ave} = 0.25$–0.35. This is in the range of experimentally observed values of the macroscopic multi-asperity friction coefficient for most metallic alloys [5]. The reduction in the coefficient of friction at small contact sizes for wedge-like asperities is a result of the friction stress τ_{ave} being limited by the adhesive strength τ_{max} for small contacts, while the contact pressure continually increases with decreasing contact size due to the indentation size effect. As in figures 4(*b*) and 5(*a*), μ_{ave} decreases with increasing a (at large values of a) for the $h = 2\,\mu$m films due to the continued increase in the indentation pressure with increasing a in these thin films.

Thus, the size dependence of the single asperity friction coefficient μ_{ave} is strongly dependent on the asperity shape: according to our calculations it can either increase or decrease with a depending on the asperity shape. The indentation and sliding material length scales l_d and l_s, respectively, in the model of Bhushan and Nosonovsky [10] can be adjusted to give results similar to those obtained here. In particular, the choice $l_d > l_s$ predicts that the friction coefficient decreases with decreasing a while $l_d < l_s$ predicts the opposite. However, the physical interpretation of the length scales in the Bhushan and Nosonovsky [10] model is quite different from those in the discrete dislocation plasticity analyses. In particular, l_s in [10] is

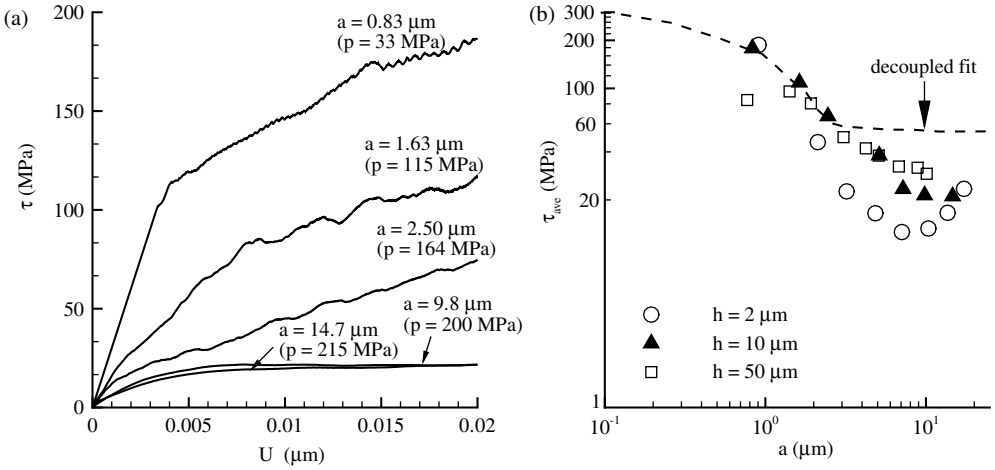

Figure 6. Effect of preceding indentation on friction. (*a*) Friction stress versus displacement response for the $h = 10\,\mu$m film (the indentation pressures for each a are indicated). (*b*) Average friction stress τ_{ave} as a function of contact size. The fit through results of figure 3(*b*) is included for comparison purposes. In these calculations the films were first indented with the $\Delta = 0.5\,\mu$m, $\lambda = 20\,\mu$m sinusoidal asperity and then sliding was initiated with the indentation pressure according to figure 2(*a*) held fixed.

associated with the mean length over which a dislocation climbs. Climb of dislocations is not accounted for in our analyses. Rather, the size dependence in the calculations here is a result of the effects of geometrically necessary dislocations, source limited plasticity and any length scale associated with the asperity.

4.4. Effect of an initial dislocation and stress state

Here we investigate the effects of the dislocation structure created by the indentation process and the stress state arising from the applied normal load on the predicted values of the friction coefficient μ.

The computed shear stress τ versus displacement U curves for selected values of the contact size a are shown in figure 6(*a*) for the $h = 10\,\mu$m films with the $\lambda = 20\,\mu$m sinusoidal asperity. A comparison with the results in figure 3(*a*) shows that (i) for large contacts ($a \geqslant 10\,\mu$m) the variation of τ with a is much like that in figure 3(*a*) and a steady-state sliding stress τ_{ave} is attained, albeit at a lower value and (ii) no distinct steady-state sliding stress is obtained for the smaller contacts ($a < 9\,\mu$m) over the range of U considered. For the larger asperity sizes, the friction coefficient, obtained by dividing τ by the values of p shown in figure 6(*a*), reaches a near steady-state value at a displacement U similar to that in figure 3(*a*). Also, the contact sizes in figure 6(*a*) are larger than those in section 4.1 and the dislocation source limited regime where τ is set by the cohesive strength is not seen.

The size dependence of the average friction stress τ_{ave} is summarized in figure 6(*b*) (for the $\lambda = 20\,\mu$m sinusoidal asperity) where again τ_{ave} is defined as the average of the shear traction τ over a displacement range $0.015\,\mu\text{m} \leqslant U \leqslant 0.02\,\mu$m whether or not a steady-state is attained. For comparison purposes, the best fit line through the results in figure 3(*b*) is also included. As in section 4.1, τ_{ave} is approximately independent of a for $a > 5\,\mu$m and increases approximately as $a^{-1/2}$ below this contact size. While the predictions of the friction stress τ_{ave} with and without an initial stress state and dislocation structure are

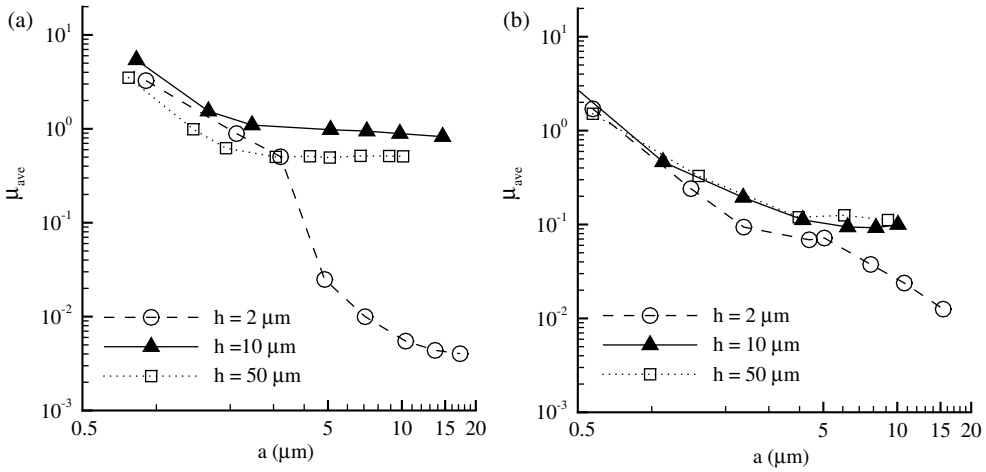

Figure 7. The scaling of the friction coefficient $\mu_{ave} \equiv \tau_{ave}/p$ with contact size a for a sinusoidal asperity with amplitude $\Delta = 0.5\,\mu$m and wavelengths (*a*) $\lambda = 20\,\mu$m and (*b*) $\lambda = 10\,\mu$m. These results are from sequential indentation and sliding calculations.

almost identical for intermediate values of contact sizes, $1\,\mu\text{m} < a < 4\,\mu\text{m}$, the values of τ_{ave} obtained here are lower for large contacts. The two main factors that contribute to this reduction in the value of τ_{ave} on the lower plateau are (i) the applied indentation force permits dislocation glide on the $\phi = \pm 54.7^\circ$ slip systems at a lower value of applied shear stress and (ii) the dislocation structure induced during indentation may also aid the sliding. Another difference between the two sets of calculations is that the average friction stress τ_{ave} in figure 7(*b*) is smaller for the $h = 2\,\mu$m film especially at large values of a whereas in figure 3(*b*) τ_{ave} is relatively independent of film thickness. This difference is rationalized by noting that typically much larger indentation forces are applied to the $h = 2\,\mu$m film to achieve a given value of a than for the thicker films. This greater indentation force (and resultant larger resolved shear stresses on the $\phi = \pm 54.7^\circ$ slip systems) reduces the shear stresses required to initiate sliding when the stress state induced by indentation is accounted for.

The predictions of the friction coefficient $\mu_{ave} \equiv \tau_{ave}/p$ are summarized in figures 7(*a*) and 7(*b*) for the $\lambda = 20\,\mu$m and $10\,\mu$m asperities, respectively. A comparison with the equivalent predictions in figures 4(*b*) and 5(*a*) shows that the two types of calculations predict similar values of μ_{ave} for the $h = 10$ and $50\,\mu$m films. However, the calculations in figure 7 predict a more dramatic reduction in the value of μ_{ave} at large a for the $h = 2\,\mu$m film due to the lower values of τ_{ave} and high values of p for a given a.

While both sets of calculations predict reasonably similar values of μ_{ave}, it is worth investigating the differences in the dislocation structures and deformation fields. The dislocation structures for both types of calculations in the $h = 50\,\mu$m film for a $a = 1.5\,\mu$m contact ($\lambda = 10\,\mu$m sinusoidal asperity) at a shear displacement $U = 0.02\,\mu$m are shown in figures 8(*a*) and (*b*). The structures are very different with the calculations starting from a stress and dislocation-free state predicting that (consistent with the findings of Deshpande *et al* [11]) dislocations are confined to a thin strip adjacent to the top surface of the film. On the other hand, with the initial stress state and dislocation structure from indentation, the dense and extensive dislocation structure created by the indentation process [13] persists during sliding which results in the dislocation structure in figure 8(*b*) differing dramatically from that in figure 8(*a*).

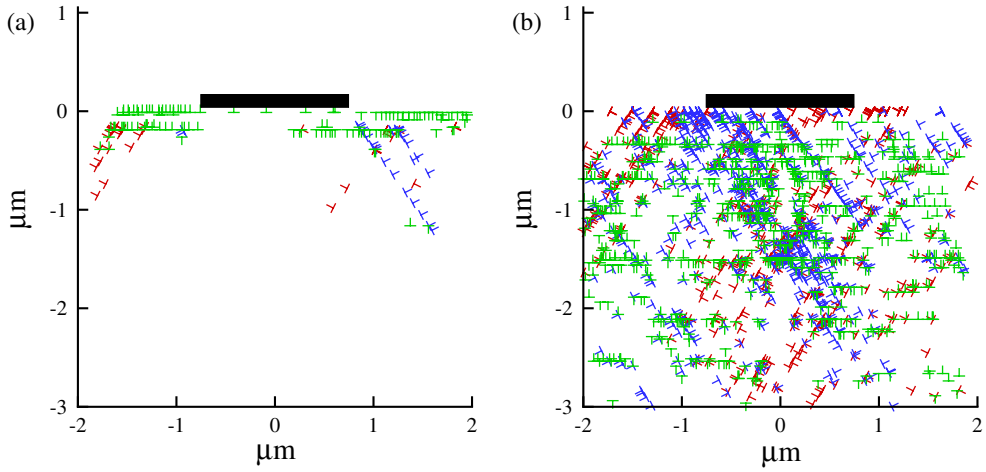

Figure 8. The dislocation structures in the $h = 50\,\mu$m film at a shear displacement $U = 0.02\,\mu$m for (a) pure sliding and (b) indentation with the $\Delta = 0.5\,\mu$m and $\lambda = 10\,\mu$m sinusoidal asperity followed by sliding. The contact zone of length $a = 1.5\,\mu$m is indicated in both cases.

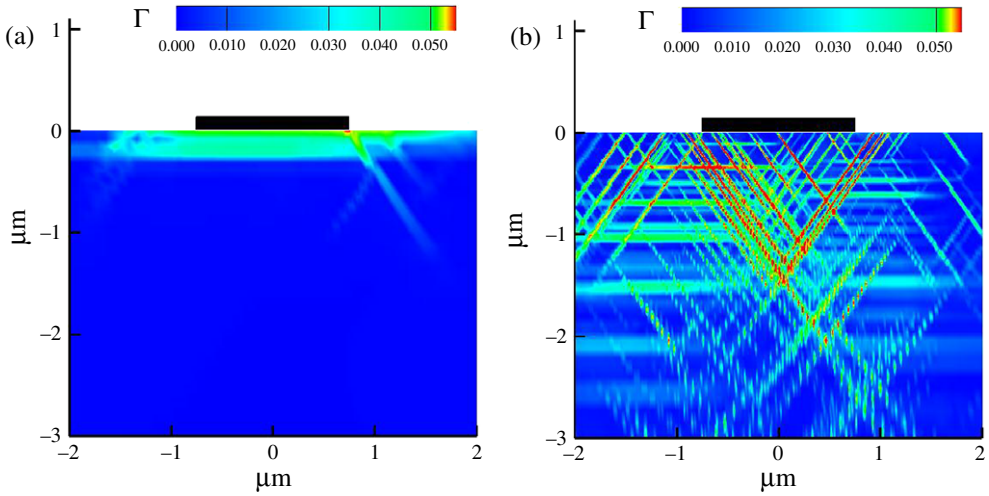

Figure 9. The distribution of the total slip Γ in the $h = 50\,\mu$m film at a shear displacement $U = 0.02\,\mu$m for (a) pure sliding and (b) indentation with the $\Delta = 0.5\,\mu$m and $\lambda = 10\,\mu$m sinusoidal asperity followed by sliding. The $a = 1.5\,\mu$m contact zone is indicated in both cases.

The corresponding slip distributions are plotted in figures 9(a) and (b) and are computed by numerical differentiation of the displacement fields u_i using the finite element shape functions. This procedure smears-out the intrinsic dislocation discontinuities over single elements and hence the absolute numerical values of Γ are not meaningful: rather Γ is only used to visualize the deformations. Consistent with the dislocation structures in figure 8, slip in figure 9(a) is confined to a narrow strip adjacent to the contact while in figure 9(b) slip spreads to at least 3 μm beneath the contact. Although the dislocation and deformation fields in the two types of calculations are significantly different, the predicted values of the friction coefficient differ little (at least for the cases considered here).

5. Concluding remarks

Indentation and sliding discrete dislocation plasticity analyses were carried out to investigate the initiation of frictional sliding between a rigid asperity and a single crystal film. Two types of sliding calculations have been carried out; in one case, sliding occurs in an initially stress and dislocation-free crystal, while in the other case there is a stress and dislocation state resulting from the preceding indentation. Plastic flow arises from the collective motion of dislocations which nucleate from initially present internal Frank–Read sources. Adhesion between the asperity and the crystal is modelled using a shear cohesive law.

- The indentation pressure versus contact size relation is dependent on the asperity shape.
- For both sets of calculations, plasticity dominates at large contact sizes and the friction stress is approximately equal to the flow strength of the crystal. At small contact sizes, the friction stress is dominated by adhesion. For intermediate contact sizes, the friction stress is contact size dependent.
- The friction stress versus contact size relation of the thicker films ($h = 10$ and $50\,\mu$m) is not significantly affected by prior indentation of the films.
- The scaling of the friction coefficient with contact size (or indentation force) is strongly dependent on the asperity shape.
- Both sets of calculations predict similar values of the friction coefficient for the $h = 10$ and $50\,\mu$m films even though the predicted deformation fields and dislocation structures are significantly different.

Acknowledgments

VSD acknowledges support from the EPSRC, UK. AN is grateful for support from the Materials Research Science and Engineering Centre at Brown University (NSF Grant DMR-0520651).

References

[1] Dieterich J 1979 *J. Geophys. Res.* **84** 2161–8
[2] Ruina A 1983 *J. Geophys. Res.* **10** 10359–70
[3] Prakash V and Clifton R 1993 *Proc. 7th Int. Congr. on Experimental Mechanics (Las Vegas, NV, USA)* (Bethel, CT : Society of Experimental Mechanics) pp 556–64
[4] Gearing B, Moon H and Anand L 2001 *Int. J. Plast.* **17** 237–71
[5] Bowder F and Tabor D 2001 *The Friction and Lubrication of Solids* (Oxford: Clarendon)
[6] Kuhlmann-Wilsdorf D 1981 *Fundamentals of Friction and Wear of Materials* (Materials Park, OH, USA: ASM) pp 119–86
[7] Polonsky I and Keer L 1996 *Proc. R. Soc. Lond. Ser. A-Math. Phys. Eng. Sci.* **452** 2173–94
[8] Hurtado J and Kim K 1999 *Proc. R. Soc. Lond. Ser. A-Math. Phys. Eng. Sci.* **455** 3363–84
[9] Hurtado J and Kim K 1999 *Proc. R. Soc. Lond. Ser. A-Math. Phys. Eng. Sci.* **455** 3385–400
[10] Bhushan B and Nosonovsky M 2003 *Acta Mater.* **51** 4331–45
[11] Deshpande V, Needleman A and Van der Giessen E 2004 *Acta Mater.* **52** 3135–49
[12] Van der Giessen E and Needleman A 1995 *Modelling Simul. Mater. Sci. Eng.* **3** 689–735
[13] Balint D, Deshpande V S, Needleman A and Van der Giessen E 2006 Discrete dislocation plasticity analysis of the wedge indentation of films *J. Mech. Phys. Solids* **54** 2281–303
[14] Homola H, Israelachvlli J, McGuiggan P and Gee M 1990 *Wear* **136** 65–83
[15] Carpick R, Agrait N, Ogletree D and Salmeron M 1996 *J. Vac. Sci. Technol.* B **14** 1289–95
[16] Li Q and Kim K S 2006 Size dependence of friction, in preparation
[17] Luan B and Robbins M 2005 *Nature* **435** 929–32
[18] Yang J and Komvopoulos K 2005 *J. Tribol.—Trans. ASME* **127** 513–21
[19] Ruan J and Bhushan B 1994 *J. Tribol.—Trans. ASME* **116** 378–88
[20] Nix W and Gao H 1998 *J. Mech. Phys. Solids* **43** 411–23